ChemPhysChem, accepted (2009)

How does the *trans–cis* photoisomerization of azobenzene take place in organic solvents?

Giustiniano Tiberio, Luca Muccioli, Roberto Berardi and Claudio Zannoni*

Dipartimento di Chimica Fisica e Inorganica and INSTM, Università di Bologna ,viale Risorgimento 4, IT-40136 Bologna, Italy

* Fax: +39 051 644 7012, E-mail: Claudio.Zannoni@unibo.it

Abstract

The *trans–cis* photoisomerization of azobenzene–containing materials is key to a number of photomechanical applications, but the actual conversion mechanism in condensed phases is still largely unknown. Here we have studied the (n, π^*) isomerization in vacuum and in various solvents via a modified molecular dynamics simulation adopting an *ab initio* torsion–inversion force field in the ground and excited states while allowing for electronic transitions and for a stochastic decay to the fundamental state. We have determined the *trans–cis* photoisomerization quantum yield and decay times in various solvents (*n*–hexane, anisole, toluene, ethanol and ethylene glycol), obtaining results comparable with the experimental ones where available. We find a profound difference between the isomerization mechanism in vacuum and in solution, with the often neglected mixed torsional–inversion pathway being the most important in solvents.

Keywords

Azo compounds, Isomerization*, Molecular Dynamics*, Photoresponsive Materials, Actuators, Atomistic Simulation*
(basic keywords*)

1 Introduction

It is well known that AB and its derivatives can undergo a major structural change upon irradiation with light, transforming from the longer *trans*–isomer to the shorter, bent, *cis*–isomer and vice versa. This variation, coupled with the high stability of the *cis* form and the reversibility of the isomerization,

can be exploited in the design of materials with photo–switchable physical properties [1, 2, 3, 4] for photonic [5] and micro– and nano–scale device applications [6, 7, 8, 9, 10, 11, 12]. Understanding the molecular mechanism of the *trans-cis* conversion and how it can take place in the crowded environment of a condensed phase is thus a task of great importance but also one of considerable complexity that still awaits to be clarified. This is not surprising, since the simulation of photoisomerization, which includes excited states dynamics and nonadiabatic crossings between different electronic states has been challenging computational chemists and physicists [13, 14, 15, 16] since many years, even in the gas phase. In particular, notwithstanding the considerable progress of quantum chemical excited state methods in the investigation of potential energy surfaces (PES) and of their intersections [17], in nonadiabatic dynamics techniques [18, 19, 20, 21, 22], a fully quantum chemical simulation [23] of a photochemical process in a complex environment and at given thermodynamic conditions is still not feasible. In the search of a suitable approximation that reduces the computational burden to amenable levels, a number of proposals for treating various contributions to the total hamiltonian at different levels of theory have been put forward. For example in the QM/MM approach some atoms, usually belonging to the solvent [24, 25, 26] or to the non-active part of a large molecule[27, 28] are treated classically, while in the molecular-mechanics valence bond method [29] and in the tight binding density functional theory [30] the subdivision regards the electrons on each atom. Also more affordable semi-empirical hamiltonians, suitably parametrized by means of higher level calculations, have been employed to describe the dynamics of a chromophore [31, 32, 33], with considerable advantages in terms of computational time, while the interaction with the surrounding environment is again modeled with classical force fields.

However, a further drastic simplification is needed to be able to study the photochemistry of complex systems with adequate sampling and time scales, and it would be desirable to extend to excited states the application of classical force fields, that have proved to be successful in describing and predicting ground state physical properties. While is certainly becoming possible for phenomena which are determined by the excited states equilibrium geometries, such as steady emission spectra [34], since in principle they can be described as accurately as the ground one with molecular mechanics, the classical description of dynamics processes that take place upon photon absorption is by far more complicate, given the large displacements from the excited state equilibrium geometry that can follow a Franck-Condon transi-

tion from the ground state. It is also worth noting that the curvature of the potential energy surface (PES) along these displacement coordinates is hardly representable with harmonic functions of normal modes. In this context, it has proved helpful to select the vibronic channels relevant for the dynamics [35, 36] and treating them at quantum mechanical level, while adopting a more approximate descriptions for the less relevant ones.

On the positive side, the AB photophysics at the root of the conformational change has been extensively studied for fifty years, and various essential features are now understood, at least in the gas phase. The process, that typically occurs in the picosecond time scale, can involve a (n, π^*) or a (π, π^*) absorption, depending on the excitation wavelength [31, 37, 38, 39]. In the most common experimental conditions (a near UV excitation), a three–state mechanism seems to take place, with promotion from the fundamental state S_0 of the *trans* isomer to the second singlet excited state S_2, followed by a decay to the first singlet state S_1, and finally by a decay, either non–radiative via conical intersection (S_0/S_1 CI) or radiative by weak fluorescence, to the S_0 state. The process can be even more complex and some authors have recently pointed out the importance of other singlet and triplet states [31, 40, 41, 42]. By comparison, the photophysics of the process following the (n, π^*) absorption from the ground state in the visible ($\lambda = 440 - 480$ nm) is simpler as it involves only the first excited state S_1 [39, 43, 44]. In addition to the photophysical aspects, the intramolecular mechanism of the isomerization process involves two basic pathways: torsion (changing the dihedral angle *Ph-N=N-Ph*), that requires a reduction of the order of the nitrogen-nitrogen double bond, and inversion, that implies a wide increase of the *Ph-N=N* bending angles with an exchange of the position of the lone pair of one of the nitrogens. The two mechanisms have often been considered in alternative, and their relative contributions to the isomerization is still controversial even in the gas phase, although some precious clarification has been provided by recent works [31, 41]. In the more general case the photoactive molecule can be considered to undergo a mixed mechanism that involves both processes and that reduces to pure torsion or inversion only in the limiting cases. Surprisingly enough the *trans–cis* quantum yield for the (n, π^*) is nearly double than that of the (π, π^*) in *n*–hexane [45], while according to the standard wisdom (Kasha rule) they should be the same. This violation seems to be generalizable to other aromatic compounds containing the nitrogen-nitrogen double bond, such as phenylazo imidazoles [46].

Given that in all practical applications the AB photoisomerization takes

place in solution or in a polymer, it is somehow disappointing that the vast majority of the theoretical information available only refers to isomerization in the gas phase, where the conformational change is not hindered by the environment and where we can expect that the mechanism can be different. As we have seen, part of the difficulty in studying the solvent environment effects on the *trans–cis* isomerization is due to the need of building a model of the process that combines the essential photophysics with an atomistic description of the guest–host system.

Here we wish to contribute to this challenging task by following the photophysically simpler (n, π^*) transition in various low molar mass organic solvents using non equilibrium molecular dynamics (MD) simulations, allowing also for transitions from the ground to the excited state and back during the time evolution. The method we propose is in essence a simple QM/MD scheme and we aim at testing the methodology as well as getting new physical insights on the mechanism of photoisomerization in organic solvents. We believe this investigation to be particularly timely, since significant experimental studies on AB photoisomerization in solution following a S_1 excitation have started to appear [39].

The paper is organized as follows: in the next section we introduce the models adopted for the AB ground and excited states, then we describe our procedure for modelling with "virtual experiments" the transitions between the two states, while parameterization details are given in Appendix. We also discuss the modelling of the various solvents and the simulation conditions. In the latest sections we describe our simulations results, discussing the isomerization mechanism, and its modifications when going from vacuum to solvents and providing a comparison with experimental data when available.

2 Models and Simulation Details

2.1 Azobenzene ground and excited states

We have modeled the AB molecule at fully atomistic level starting from the AMBER molecular mechanics force field (FF) [47], similarly to other recent studies of AB derivatives [48, 49] and modifying some terms in order to approximate *ab initio* energy profiles. The *trans–cis* isomerization directly influences at least five internal degrees of freedom [50], namely: the *Ph-N=N-Ph* torsional angle (ϕ), the two *Ph-N=N* bending angles (θ), and both *N=N*

and *Ph-N* bond lengths. Since the only QM complete PES for azobenzene available in the literature is restricted only to the two most important internal coordinates, the torsional angle ϕ and one of the bending angles θ [38], and also because of the increasing computational complexity associated to the use of manifold PES, we limit here the QM-derived force field contributions only to these two degrees of freedom. The remaining ones instead are assumed to be reasonably described, for the purpose of this study, by the AMBER FF for the ground state. We note that this simplification may possibly lead to an incorrect description of the symmetric inversion channel, a decay pathway producing the *trans* isomer which is probably responsible for the quantum yield decrease upon S_2 ($\pi\pi^*$) excitation, but should be scarcely relevant for S_1 excitation [44, 51].

According to this parameterization choice, we have replaced the standard FF torsional and bending contributions with appropriate functions of the torsional angle ϕ and of one of the bending angles θ (Figure 1) both in the ground and in the first singlet excited state. We have employed as far as possible the *ab initio* CASSCF (θ, ϕ) potential energy surfaces for the two electronic states S_0 and S_1 obtained by Ishikawa *et al.* [38]. Since the numerical value were not available we have sampled the published data with uniform grid of 10×10 points in the range $105° \leq \theta \leq 180°$ and $0° \leq \phi \leq 180°$, and approximated the $0° \leq \theta \leq 105°$ region with least square parabolas fitting the grid points in the $105° \leq \theta \leq 110°$ range. During the simulation, the standard bending and torsional contributions for θ and ϕ are then replaced by second order Lagrange interpolation over the grid points, that is used to compute energies and forces for arbitrary (θ, ϕ) values,

It should be noted that in the quantum mechanical PES all intramolecular electrostatic and dispersive interactions between the AB atoms are implicitly included. To correct the FF, and thus avoiding counting these terms twice when the standard sum over charges and atoms is performed in the MD simulation [52], we have subtracted from the *ab initio* PES $U^{ai}_{S_n}(\theta, \phi)$ for the n=0,1 states the molecular mechanics one $U_c(\theta, \phi)$, calculated with zeroed explicit bending terms for θ and torsional for ϕ. In practice, to evaluate the required contributions we have preliminarily sampled the distribution $f_c(\theta, \phi)$ by performing a constant volume, 10 ns–long MD simulation of an isolated AB molecule at $T = 2000$ K; such a high temperature has been chosen to guarantee a thorough exploration of the PES during the trajectory. We have then obtained the correction $U_c(\theta, \phi)$ to the total conformational energy

through an inversion of the distribution as in reference [53]

$$U_c(\theta, \phi) = -k_B T \ln f_c(\theta, \phi) - U_0, \tag{1}$$

where k_B is the Boltzmann constant and U_0 shifts to zero the minimum of the energy. The corrected force field contribution for the state S_n is therefore:

$$U_{S_n}(\theta, \phi) = U^{ai}_{S_n}(\theta, \phi) - U_c(\theta, \phi) \tag{2}$$

and replaces the torsional term for the *Ph-N=N-Ph* dihedral and the bending term for the *Ph-N=N* angle.

2.2 Azobenzene excitation and decay

To perform during the MD simulation the virtual excitation and decay experiments, we imagine the system to be exposed to radiation of the suitable wavelength. The transition between the electronic states has been modelled in a simplified way, by considering the $S_0 \rightarrow S_1$ process to take place within the Franck–Condon regime, i.e. as a vertical transition occurring at fixed nuclei positions. We have scheduled an excitation event (photon absorption) at regular time intervals of 10 ps along the ground state trajectory which proceeds in the background. When this happens, the FF parameterization for the AB molecule is switched from that of the ground state S_0 to that of the first excited state S_1 and a new and independent MD trajectory is spawned from the main one.
This secondary trajectory is then followed while AB moves and changes its conformation according to the S_1 PES and under the influence of the solvent environment and eventually decays back and relax in S_0. The probability of nonradiative decay to the ground state ($S_1 \rightarrow S_0$) has been modeled statistically according to an energy gap law [54, 55]:

$$dP_{1\rightarrow 0}(\theta, \phi, t)/dt = K \exp\left\{-\chi[U_{S_1}(\theta, \phi) - U_{S_0}(\theta, \phi)]\right\}, \tag{3}$$

where $U_{S_1}(\theta, \phi)$ and $U_{S_0}(\theta, \phi)$ are respectively the energies for the excited and ground state in the given (θ, ϕ) conformation (see Equation 2), $P_{1\rightarrow 0}(\theta, \phi, 0) = 0$, and χ (1.5 and 1.9 mol kcal^{-1} in vacuum and solvents), K (5 fs^{-1}) are empirical constants whose estimation is described in the Appendix. The probability of occurrence of the inverse process ("recrossing" from the S_0 to the S_1 surface) was instead neglected in the simulation.

This simple model for non-radiative decay, originally due to Jortner [55], is now widely accepted and supported by many theoretical and experimental studies [54, 56, 57], even though it is not applicable to all systems [58]. The energy gap law approximation seems here somehow justified by the fact that the conical intersection lies very close to the minimum of the excited state and to the maximum of the ground state PES, therefore it can be considered as a "minimum energy" CI, i. e. the centre of a broad region where population transfer may occur [21]. Is is worth mentioning that at least other two conical intersections with the ground state are present on the S_1 PES, but only the minimum energy one modelled here is likely to be accessible through n, π^* excitation, whilst the others become important when reaching the S_1 state from higher excited states ("hot" isomerization) [40, 41, 44, 51, 42].
In practice, during each trajectory in S_1 a uniformly distributed random number was generated every time step and the transition to the fundamental state was accepted or not using Equation 3 and applying von Neumann's rejection method [59].

2.3 Solvents and solutions

We have studied the *trans–cis* isomerization of AB either isolated (in vacuum, VAC) or dissolved in five isotropic solvents: *n*–hexane (HEX), also employed to parameterize the decay model of Equation 3, as well as anisole (ANI), ethanol (ETH), ethylene glycol (EGL), and toluene (TOL). The five solvents have a different density, viscosity and polarity (see Table 1) and later on we shall try to connect these features to their effects on the isomerization process. For all the compounds studied (AB in S_0 and solvents) we have preliminarily performed a quantum mechanical DFT B3LYP/6–31G** geometry optimization, and determined the atomic point charges using the ESP scheme with the additional constraint of reproducing the total dipole moment [60]; their values were kept fixed during all simulations.

We have further assumed the AB intramolecular energy for torsion anx bending (Equation 2) to be unaffected by solute–solvent interactions. This necessary, even if seemingly drastic, approximation is supported theoretically and experimentally at least in terms of the scant variation of vertical excitation energies registered in different solvents [61, 45, 62, 63]. On the other hand the intermolecular (van der Waals and electrostatic) AB-solvent interactions are taken into account and greatly affect the *trans–cis* conversion as

shown later. In particular, the explicit consideration of atomic charges, albeit in an approximate way, allows us to start to investigate solvent polarity effects.

2.4 Simulation conditions

Each sample consisted of one *trans*–AB molecule surrounded by 99 solvent molecules, all modelled at atomistic level, and contained in a cubic volume with three-dimensional periodic boundary conditions (PBC). We have found this relatively small sample size to be sufficient to describe about two solvation shells, and thus adequate for the short range solvent effects expected in these isotropic systems. The simulations have been conducted with a in-house modified version of MD code ORAC [64], integrating the equations of motion with a multiple time step scheme[64] with longest time step $\Delta t = 5$ fs. Electrostatic long-range interactions were evaluated with the Particle Mesh Ewald method [65], with parameters $\alpha = 0.4$ Å^{-1}, a cubic grid of size 30 and 4^{th} order splines. Simulations were kept in isothermal–isobaric conditions (NPT) using a Nosé–Hoover thermostat [66, 67], and an isotropic Parrinello–Rahman barostat [68] at the pressure of 1 atm and $T = 300$ K. The simulations in vacuum were performed for AB in a cubic box with sides of 100 Å and canonical (NVT) conditions at $T = 300$ K. The MD equilibration was continued until specific thermodynamics observables (e.g. density, energy) were found to fluctuate around a constant average value for at least 1 ns. In Table 1 we see that the equilibrium densities obtained for the five solutions compare rather well with the corresponding experimental values for the pure solvents.

After this preliminary stage, we have used the equilibrated samples to follow for 15 ns the main trajectories described earlier. The configurations used as starting point for the virtual excitation-decay experiments were extracted every 10 ps, for a total of 1500 independent measurements for each system (vacuum and solvents). After the vertical electronic transition $S_0 \rightarrow S_1$, the ensuing relaxation dynamics was followed with NVT simulations for a time window (VAC 10 ps, EGL 150 ps, for other solvents 50 ps) wide enough to span both the experimental isomerization time scale and the solvent-dependent relaxation times. Figure 2 provides a graphical representation of a typical trajectory. As each experiment provides a different estimate of the permanence time in the excited state, determined by the statistical sampling of the hopping probability $P_{1\rightarrow 0}$ (integrating equation 3 as

$P_{1\to0}(\theta,\phi,\Delta t) = \Delta t\ K \exp\{-\chi[U_1(\theta,\phi) - U_0(\theta,\phi)]\}$, with $\Delta t = 5$ fs), a large number of excitation events was necessary to compute the ensemble–averaged observables which are presented in the following.

3 Results and discussion

3.1 Quantum yields and lifetimes

We start analysing the *trans-cis* AB quantum yields obtained from $N = 1500$ independent experiments in vacuum and solvents; these values are directly compared in Table 2 with the experimental ranges reported, following the classification of polar, protic and viscous solvents introduced in [69]. All computed yields in solvent are very similar; this is not surprising as it is experimentally known the very weak dependence of Φ on solvent properties, in particular from the work Fischer and coworkers [70, 71]. All yield values fall in the experimental range except the one in EGL, which is also somehow at variance with $\Phi = 0.43$ in glycerol registered by Fischer and coworkers [71]. What is striking is the strong reduction of the yield in solvent with respect to vacuum: as we shall show later (and can be intuitively deduced from Figure 1), for a successful photoisomerization the specific shape of PES determines that torsional angles lower than about 90 degrees have to be reached, starting from the Frank-Condon point at 180 degrees. The solvent hindrance slows down the motion in the excited state (cf S_1 lifetimes in Table 2) thus increasing the probability of decaying at higher torsional angles, and consequently of going back to a ground state *trans* isomer. It is worth noting that a similar result was obtained by Creatini et al. in a surface hopping simulation in vacuum, where the solvent effect was mimicked with a pulling force [72]. Their study, which makes use of a more sophisticated decay probability law than ours, shows that the quantum yield always decreases when the force is applied, and that the isomerization pathway remains predominantly torsional nonetheless. The excited state lifetimes τ_{S_1} are weakly affected by solvent properties and in all instances fall in the picosecond time scale. However, in the case of EGL viscosity, which is one order of magnitude larger than for the other solvents studied here, determines a significantly longer lifetime. Such an effect has already been reported for the π,π^* isomerization of the azo dye Disperse Red 1, in which τ_{S_1} goes from 0.9 ps in ANI to 1.5 ps in EGL [73], but also for azobenzene n,π^*

isomerization by Chang et al. (in HEX $\tau_1 = 0.24 - 0.33$, $\tau_2 = 1.7 - 2.0$ ps; in EGL $\tau_1 = 0.35 - 0.65$, $\tau_2 = 3.1 - 3.6$ ps) [39]. Also the MD result in ETH is in good agreement with time-resolved measurements for azobenzene ($\tau_1 = 0.32$, $\tau_2 = 2.1$ ps) [74] and 4-aminoazobenzene ($\tau_1 = 0.5 - 0.6$, $\tau_2 = 1.7 - 2$ ps)[75]. The S_1 population decay is clearly not mono-exponential in vacuum, and to a lesser extent in solvents (Figure 3). For attempting a comparison with time-resolved experimental decays, and for sake of reproducibility, in Table 2 we report the results of a fit of a delayed biexponential function $P_{S_1}(t) = a_1 \exp(-(t - \tau_0)/\tau_1) + a_2 \exp(-(t - \tau_0)/\tau_2)$ to the excited state population; in all cases we obtained a higher coefficient for the slowest decay component. Simulations also allow to compute separately excited state lifetimes for successful and unsuccessful isomerization outcome, however in Table 2 we show that they are not distinguishable, at least with the number of experiments we performed, suggesting the possibility of a unique S_1 pathway.

Concluding the discussion on lifetimes, we would like to attempt a direct comparison with fluorescence time-resolved experiments: in Figure 4 we show the time evolution of emission at $\lambda = 680$ nm published in [39] for hexane and ethylene glycol, together with the probability of the $S_1 - S_0$ energy gaps calculated from our simulation for three different wavelengths, and finally the excited state population. More than discussing the agreement between simulation and experiment, which for many reasons is very difficult to judge (for example in the simulation the fluorescence probability was assumed constant in time, and the pulse shape is a Dirac's delta), the comparison between the excited state population and the simulated emission is very interesting, as it clearly shows that they are very different, even if of course related; in particular when increasing the sampling wavelength the intensity peak of the emission appears progressively delayed with respect to the time origin (vertical excitation); moreover sampling a single wavelength seems to cause a decrease of the long time component, and the decay time τ_{S_1} is consequently always underestimated by the fluorescence experiment. As a side comment we would like to underline that, besides the knowledge of AB transition dipole as function of the molecular geometry [63], a good statistics is needed to simulate this type of observable (cf the noise in Figure 4), as at any time value only the small fraction of molecules which is still excited and lies in a specific region of the PES contributes to the histogram.

3.2 Geometry modifications during the isomerization process

Having seen that our simulations can reproduce semi-quantitatively quantum yield and decay time data, we now wish to focus on the details of the *trans–cis* transformation in solution as obtained from our computer simulation results. We have monitored the isomerization mechanism with various geometrical indicators, related to the structural reorganization of AB, including the absolute value of the *Ph-N=N-Ph* torsional angle ($|\phi|$), the selected *Ph-N=N* bending angle (θ), the distance between the outmost $4, 4'$ carbons of the phenyl rings ($r_{4,4'}$), and the average module of the four *Ph-N=N* torsional angles ($|\gamma|$) which monitors the rotation of the phenyl groups. The dynamic evolution of these indicators from the initial *trans* values is reported in Figure 5, where for clarity we do not plot the curves in anisole and toluene since they are very similar to those in hexane. The averages have been computed considering all the experiments and separating the values for the trajectories leading to successful (*cis* final isomer) and unsuccessful (*trans* final isomer) photoisomerization outcomes, as indicated by the lateral bars on the right edges of the plots of Figure 5. We first notice that the AB isomerization in vacuum differs from the one in solution in that the trajectories are already well separated at 0.5 ps in two branches leading to *cis* and *trans*. For all other cases we can observe, looking at Figures 5–[a], 5–[c] and 5–[d], that the geometrical indicators in the excited state (first few picoseconds) are still closer to those of the starting *trans* isomer than those of the *cis*. The exception to this pattern is given by the bending angle (Figure 5–[b]), which within the first 0.5 ps in the excited state has already attained values closer to the *cis* conformer ones.

We can see that the *trans–cis* isomerization involves a large rotation of a phenyl group from $|\gamma| = 4 - 10°$ to $|\gamma| = 30 - 40°$ (and even larger in vacuum) and thus if this rotation is hindered, e.g. by steric interactions with the neighboring solvent molecules, the isomerization dynamics is correspondingly slowed down (Figure 5–[d]), and the quantum yield consequently decreases. The distance indicator $r_{4,4'}$ is strictly related to the torsional angle ϕ (see Figures 5–[a] and 5–[c]) and shows directly the overall shortening of the AB when going from the *trans* to *cis* conformer, that turns out to be about 2.25 Å in solution and 2.5 Å in vacuum. Recalling the permanence times in the excited state (Table 2), it can be safely concluded that most of the geometrical rearrangements take place (or continue for a long time) in the ground state,

while in the excited state both unsuccessful and successful trajectories are very similar, indicating a unique pathway in the S_1 PES like suggested by other studies [31].

The rotational dynamics of AB, which has been sometimes brought into play in the interpretation of time–resolved experiments [39], can also be followed by MD simulations [76]; here we chose to monitor it through the time autocorrelation function of the unit vector describing the orientation of the -N=N- bond, $\langle \mathbf{r}_{NN}(0) \cdot \mathbf{r}_{NN}(t) \rangle$ in Figure 6. These functions clearly show that the rotation of the molecule takes place on a longer time scale than that of the isomerization process, with typical times depending on the solvent and on the isomerization product. To better quantify these effects, we estimated the rotational correlation times τ_r as the time at which $\langle \mathbf{r}_{NN}(0) \cdot \mathbf{r}_{NN}(\tau_r) \rangle = 1/e$ (Table 3) and displayed in a log-log plot versus experimental viscosities (Figure 7). To investigate the dependence of rotational times τ_r and lifetimes τ_{S1} on solvent experimental viscosities, we interpolated both data sets with a power law, commonly used in the analysis of time–resolved fluorescence data [77]:

$$\tau_r^{-1} \; = \; A\eta^{-\alpha}. \tag{4}$$

All times were well fitted with this equation but the ones in ethanol, probably because our simulations do not seem to reproduce correctly the actual viscosity value for this solvent. The rotational times of the N=N axis exhibit a Stokes-Einstein like behaviour, i.e. they are roughly proportional to solvent viscosity ($\alpha \approx 1$), but they are clearly separated in two groups, one for the *trans* and one for the *cis* final isomer. As expected the shape of the molecule affects the rotational dynamics, but quite surprising is the outcome for AB isomers, in fact the *trans* rotates about the N=N vector approximately two times faster than the *cis*; we believe that this physical effect should be taken into account in the interpretation of time-resolved measurements.
The excited state lifetimes show a different behaviour: they are weakly affected by the viscosity ($\alpha = 0.2$), in accord with experimental results of an AB acrylate derivative [78], and as previously observed, they do not apparently depend on the final isomerization product; consequently the data sets for *cis* and *trans* AB can be fitted with the same set of parameters.

3.3 Isomerization mechanism

We now proceed to assess the likelihood of the torsion or inversion *trans–cis* isomerization channels by following the molecular geometry time evolution. To do this, we have first defined three main isomerization pathways in the (θ, ϕ) surfaces according to the upper limit, θ_{max}, of the bending angle values explored by the AB molecule during its trajectory in both electronic states: *torsion* (if $\theta_{max} < 140°$); *mixed* (if $140° \leq \theta_{max} < 160°$); and *inversion* (if $\theta_{max} \geq 160°$); then, we have classified each experiment according to this definition and evaluated the relative importance of each of the channels computing the ratios reported in Table 4.
two most probable pathways for isomerization are the torsional (56%) and mixed ones (43%), with unlikely occurrence of pure inversion, in agreement with other semiclassical studies [31, 79]. We also find that, even if the ratios exhibit different values in the various solvents, the most probable pathways in condensed phase always correspond to a mixed mechanism [80]. Pure inversion and pure torsional pathways seem to be hindered by steric solvent interactions and are consequently less likely to occur. Even if we registered the highest occurrence of inversion pathways in the more viscous solvent (ethylene glycol), in agreement with reference [39], the isomerization mechanism seems relatively unaffected by solvent viscosity.

In their recent QM/MM study on *cis-trans* isomerization of AB, where both AB PES and excited state dynamics were treated at DFT level, Marx and coworkers [80] evidenced that the isomerization mechanism somehow departs from the standard torsional or inversion pathways, as it involves a faster rearrangement of nitrogen atoms with respect to the bulkier phenyl rings. In order to compare our findings with this study, we have evaluated specific autocorrelation functions measuring the time change of orientation of the normal to each phenyl ring plane ($\mathbf{n}_R$), and of the orientation of the normals to the planes containing C-N=N atoms ($\mathbf{n}_N = \hat{\mathbf{r}}_{CN} \times \hat{\mathbf{r}}_{NN}$) for successful isomerizations (Figure 8). We have found that, in line with the results in [80], a faster reorientation of $\mathbf{n}_N$ with respect to $\mathbf{n}_R$ during the isomerization for all the cases studied, as shown by the faster decay of the corresponding autocorrelation functions in Figure 8. Since our simulation are on one hand based on different (and more drastic) approximations on the photophysics, and on the other, they explore a time window up to one hundred times larger than that studied in [80], we think that these two independent approaches provide a cross-validation of the isomerization mechanism. In addition, the

availability of simulations for different solvent viscosities allows to identify the marked effect this property has on the isomerization dynamics: as expected, the bulky phenyl groups need more time to adapt their orientation to the change of PES occurring upon excitation. This effect gives rise to the predominance of what we call "mixed" isomerization mechanism in the excited state, even if the reorientation dynamics continues also after the decay to S_0.

The analysis of MD simulations trajectories also gives insights on the electronic state dependence of the inversion and rotation processes. When the molecule is excited, it generally moves torsionally towards the S_1 surface energy minimum and conical intersection region, and only after it has decayed to the S_0 state, the bending angle θ can reach values close to 180°. As evidenced by the low fraction of trajectories reaching the maximum bending angle in the excited state (Table 4), the inversion movement takes place primarily in the S_0 state, at least in these excitation conditions. These results support the "cold isomerization" model described by Diau and coworkers [81], that depicts a rotational pathway in the S_1 state for an (n, π^*) excitation. The inversion mechanism in the excited state could become possible only if the molecule started from a higher vibrational state ("hot isomerization") having enough energy to overcome the inversion energy barrier; this second mechanism is expected to be important only after a decay from a higher excited state [82], as it can happen in (π, π^*) isomerization.

4 Conclusions

In this work we have analyzed the mechanism for the *trans–cis* photoisomerization of azobenzene in various organic solvents when excited in the visible ((n, π^*) transition). For this purpose, we have introduced a method for the molecular dynamics simulation of photoresponsive molecules in solution which has the feature of allowing for their electronic excitation and statistical decay while they move in the crowded solvent environment. With the help of two empirical parameters to model the decay probability of AB from S_1 to ground state, tuned for reproducing experimental quantum yields and the excited state lifetimes in vacuum and hexane, we have been able to follow the conformational changes of AB and to evaluate conversion efficiency and decay dynamics in different solvation conditions.

The average decay times resulted fairly independent on the nature of the

photo product obtained after decay, thus indicating similar trajectories in the excited state for both possible outcomes. The simulations also show that, while in vacuum the isomerization follows prevalently a torsional mechanism, as already found by other authors [31], the dominant isomerization mechanism in solution is a mixed torsional-inversion one, with a probability which is double than the one for a pure torsion. Indeed the pure inversion seems to occur only after the decay into the S_0 state, while in the excited state this pathway appears unlikely, as a high energy barrier must be overcome. A higher solvent viscosity seems to increase the pure inversion contribution, albeit the principal mechanisms remain the mixed one and torsional ones (with a probability of about 65% and 30% respectively). Viscosity also clearly affects the rotational dynamics of AB, notably resulting in a faster dynamics for the *trans* isomer.

Addressing the interpretation of time-resolved absorption or emission experiments, we have predicted the intensity time profile to be a lower bound of the excited state population, and also suggested that the different rotational times of the two isomers must be taken into account when evaluating the depolarization of fluorescence.

Although a number of approximations have been introduced to make the study computationally feasible, we believe the present approach to be quite general, easily improvable as soon as more accurate quantum mechanics description of electronic states and transition probabilities become available, and applicable to other, even more complex, isotropic and anisotropic surroundings.

5 Acknowledgements

We acknowledge EU RT Network *"Functional Liquid Crystalline Elastomers"* (FULCE) for initially funding this research, and a CINECA-INSTM computer time co-funded grant. We also wish to thank Prof. Maurizio Persico (university of Pisa) and Prof. Giorgio Orlandi (university of Bologna) for useful discussions.

Appendix: parameterization of the decay probability law in vacuum and hexane

In this appendix we discuss the technical details for derivation of the two parameters K and χ appearing in the decay model described by Equation 3. At least in principle these parameters, or the probability rates themselves, could be calculated *ab initio*, but for simplicity here we followed an empirical approach, consisting in tuning K and χ on the basis of the comparison with available theoretical data in vacuum and experimental ones in hexane. The typical observable of a photoisomerization experiment is the quantum yield, Φ, expressing the ratio between the number of isomerized molecules and the number of absorbed photons. Richer dynamical information can be gathered with pico or femtosecond time–resolved experiments (e.g. absorbance, fluorescence, IR, Raman), which measure the time evolution of some transient species characteristic spectral features; however these results are often difficult to interpret [69, 63], as they represent a weighted average of both isomers dynamics, and they are to some extent also dependent on solvent nature, on probing wavelength and, of course, on excitation wavelength, that may determine different excited state pathways. In the case of $n\pi^*$ excitation, the intensity decay is usually well fitted with a tri-exponential function, with lifetimes τ_1, τ_2, and τ_3 of the order of magnitude of $0.1-1$, $1-5$ and $10-30$ ps respectively [81, 39, 83], and relative weight $2-3:1:<0.1$. The faster decay is reasonably ascribed to the relaxation from the Frank-Condon point to the minimum of S_1, while for the other two the assignment is more controversial; here we base the parametrization on the interpretation of the second process as the relaxation in the flatter CI region, and the third one to the rotational and vibrational cooling in S_0 [84, 42]. Simulations allow to measure directly the time evolution of the population of S_1, and its average lifetime τ_{S_1} can be directly compared with the experimental time scale of the two fastest processes in a given solvent. The timescale of the rotational motion of AB can be calculated from the autocorrelation function of a relevant molecular axis, and again compared with τ_3. Finally, we define the the quantum yield as $\Phi = N_{cis}/N$, where N_{cis} is the number of virtual experiments yielding a *cis* isomer out of the total number of experiments N, which is in turn equivalent to the number of absorbed photons. We start presenting the quantum yield and the decay kinetics of AB in vacuum and in *n*–hexane for various sets of MD experiments differing in the values of the parameters K and χ, and comparing them with available theoretical data and with experi-

mental yields in n–hexane. Without attempting a perfect match that would be inappropriate considering the various approximations made in our approach, a comparison with these data can provide a reasonable estimate for χ and K. In particular Persico and coworkers performed several simulations of azobenzene and derivatives in vacuum using prevalently surface hopping [31, 32, 69, 72] but also full multiple spawning (FMS) [85, 86]. As they refer to this second method as the most accurate, we compare our results in vacuum with the FMS ones. Luckily not only the quantum yield (0.46 ± 0.08 in [85]), but also the lifetime of the excited state t_{S_1} (about 0.5 ps) and the S_1 population in function of time can be calculated with these techniques and a thorough comparison with our simulations is possible.

From Table 5, where we report the estimated Φ and t_{S_1} in vacuum for various values of K and χ, it is apparent that with small variations of the parameters any quantum yield ranging from 0.0 to 0.6 can be reproduced; moreover, some parameter choices can lead to reasonably correct yields and lifetimes. In the selection of the best K and χ, it would be desirable to use the same set for vacuum and hexane; for this solvent n, π^* quantum yield measurements are available but due to large experimental uncertainties only the yield range is known ($\phi = 0.20 - 0.27$) [45]. Also the data for the excited-state lifetime τ_{S_1} are relatively scattered, but always in the $1 - 3$ ps range [87, 88, 81, 39, 83].

Analysing the the test results in Table 5, some trends emerge: i) as expected, lifetime increases with increasing χ and decreasing K; ii) for any K, χ pair the permanence time is roughly doubled in hexane with respect to vacuum; iii) with K fixed, the yield increases with χ for "small" χ until reaching a maximum value of about 0.55 in vacuum and 0.24 in hexane; further increasing χ determines long lifetimes and an eventual falling of the yield (at least for $K = 5$).

It is also clear that it is not possible to obtain yield and lifetimes in perfect agreement with experiment for vacuum and hexane with a unique parameterization; on the other hand it is easy to reproduce both yield and lifetime, with different combinations of K and χ. Actually it is not clear if the coupling between the two states should be solvent-independent (i. e. with the same K, χ), as calculation and experiments indicate only small bathochromic shifts [62]; considering that the best results for hexane are obtained at high K, we have decided to keep constant $K = 5$ fs^{-1} for vacuum and solutions, but to use slightly different values of χ (1.5 in vacuum and 1.9 mol kcal^{-1} in solvents). This choice gives an excellent agreement with

the S_1 population calculated by Persico and coworkers (Figure 9) for AB in vacuum, and determines the probability maps shown in Figure 10.

References

[1] H. Finkelmann, E. Nishikawa, G. G. Pereira, and M. Warner. A new opto-mechanical effect in solids. *Phys. Rev. Lett.*, 87:15501, 2001.

[2] T. Ikeda and O. Tsutsumi. Optical switching and image storage by means of azobenzene liquid-crystal films. *Science*, 268:1873–1875, 1995.

[3] Y. Yu, M. Nakano, and T. Ikeda. Directed bending of a polymer film by light. *Nature*, 425:145–145, 2003.

[4] M. Camacho-Lopez, H. Finkelmann, P. Palffy-Muhoray, and M. Shelley. Fast liquid crystal elastomer swims into the dark. *Nat. Mater.*, 3:307–310, 2004.

[5] X. Tong, G. Wang, A. Yavrian, T. Galstian, and Y. Zhao. Dual-mode switching of diffraction gratings based on azobenzene-polymer-stabilized liquid crystals. *Adv. Mater.*, 17:370–374, 2005.

[6] Y. Lansac, M. A. Glaser, N. A. Clark, and O. D. Lavrentovich. Photocontrolled nanophase segregation in a liquid-crystal solvent. *Nature*, 398:54–57, 1999.

[7] T. Hugel, N. B. Holland, A. Cattani, L. Moroder, M. Seitz, and H. E. Gaub. Single-molecule optomechanical cycle. *Science*, 296:1103–1106, 2002.

[8] I. A. Banerjee, L. Yu, and H. Matsui. Application of host-guest chemistry in nanotube-based device fabrication: Photochemically controlled immobilization of azobenzene nanotubes on patterned α-cd monolayer/au substrates via molecular recognition. *J. Am. Chem. Soc.*, 125:9542–9543, 2003.

[9] A. Buguin, M. H. L. Silberzan, B. Ladoux, and P. Keller. Micro-actuators: When artificial muscles made of nematic liquid crystal elastomers meet soft lithography. *J. Am. Chem. Soc.*, 128:1088–1089, 2006.

[10] T. Muraoka, K. Kinbara, and T. Aida. Mechanical twisting of a guest by a photoresponsive host. *Nature*, 440:512–515, 2006.

[11] M. Yamada, J.-I. Mamiya M. Kondo M, Y.-L. Yu, M. Kinoshita, C. Barrett, and T. Ikeda. Photomobile polymer materials: Towards light-driven plastic motors. *Angew. Chem. Int. Ed. Engl.*, 47:4986–4988, 2008.

[12] J. M. Mativetsky, G. Pace, M. Elbing, M. A. Rampi, M. Mayor, and P. Samorì. Azobenzenes as light-controlled molecular electronic switches in nanoscale metal-molecule-metal junctions. *J. Am. Chem. Soc.*, 130:9192–9193, 2008.

[13] F. Bernardi, M. Olivucci, and M. A. Robb. Potential energy surface crossings in organic photochemistry. *Chem. Soc. Rev.*, 25:321–328, 1996.

[14] D. R. Yarkony. Diabolical conical intersections. *Rev. Mod. Phys.*, 68:985–1013, 1996.

[15] A. W. Jasper, C. Y. Zhu, S. Nangia, and D. G. Truhlar. Introductory lecture: Nonadiabatic effects in chemical dynamics. *Faraday Discuss.*, 127:1–22, 2004.

[16] M. Garavelli. Computational organic photochemistry: strategy, achievements and perspectives. *Theor. Chem. Acc.*, 116:87–105, 2006.

[17] D. R. Yarkony. Conical intersections: The new conventional wisdom. *J. Phys. Chem. A*, 105:6277–6293, 2000.

[18] N. L. Doltsinis and D. Marx. Nonadiabatic Car-Parrinello molecular dynamics. *Phys. Rev. Lett.*, 88:166402, 2002.

[19] G. A. Worth and L. S. Cederbaum. Beyond born-oppenheimer: molecular dynamics through a conical intersection. *Annu. Rev. Phys. Chem.*, 55:127–158, 2004.

[20] X.S. Li, J. C. Tully, H. B. Schlegel, and M. J. Frisch. Ab initio Ehrenfest dynamics. *J. Chem. Phys.*, 123:084106, 2005.

[21] B. G. Levine and T. J. Martinez. Isomerization through conical intersections. *Annu. Rev. Phys. Chem.*, 58:613–634, 2007.

[22] A. W. Jasper, S. Nangia, C. Y. Zhu, and D. G. Truhlar. Non-Born-Oppenheimer molecular dynamics. *Acc. Chem. Res.*, 39:101–108, 2007.

[23] B. Lasorne, M. J. Bearpark, M. A. Robb, and G. A. Worth. Controlling s_1/s_0 decay and the balance between photochemistry and photostability in benzene: a direct quantum dynamics study. *J. Phys. Chem. A*, 112:1301713027, 2008.

[24] J. Kongsted, A. Osted, and K. V. Mikkelsen. Solvent effects on the $n \rightarrow \pi^*$ electronic transition in formaldehyde: a combined coupled cluster/molecular dynamics study. *J. Phys. Chem*, 121:8435–8445, 2004.

[25] M. Sulpizi, U. F. Röhrig, J. Hutter, and U. Rothlisberger. Optical properties of molecules in solution via hybrid TDDFT/MM simulations. *Int. J. Quantum Chem.*, 101:671–682, 2005.

[26] A. M. Losa, I. F. Galvin, M. L. Sanchez, and M. E. Martin. Solvent effects on internal conversions and intersystem crossings: The radiationless de-excitation of acrolein in water. *J. Phys. Chem. B*, 112:877–884, 2008.

[27] L. M. Frutos, T. Andruniow, F. Santoro, N. Ferre, and M. Olivucci. Tracking the excited-state time evolution of the visual pigment with multiconfigurational quantum chemistry. *Proc. Natl. Acad. Sci. U.S.A.*, 104:7764–7769, 2007.

[28] M. Boggio-Pasqua, M. A. Robb, and G. Groenhof. Hydrogen bonding controls excited-state decay of the photoactive yellow protein chromophore. *J. Am. Chem. Soc.*, 131:1358013581, 2009.

[29] M. J. Bearpark, M. Boggio-Pasqua, M. A. Robb, and F. Ogliaro. Excited states of conjugated hydrocarbons using the molecular mechanics-valence bond (MMVB) method: conical intersections and dynamics. *Theor. Chem. Acc.*, 116:670–682, 2006.

[30] T. Frauenheim, G. Seifert, M. Elstner, T. Niehaus, C. Kohler, M. Amkreutz, M. Sternberg, Z. Hajnal, A. Di Carlo, and S. Suhai. Atomistic simulations of complex materials: ground-state and excited-state properties. *J. Phys.: Condens. Matter*, 14:3015–3047, 2002.

[31] C. Ciminelli, G. Granucci, and M. Persico. The photoisomerization mechanism of azobenzene: A semiclassical simulation of nonadiabatic dynamics. *Chem.-Eur. J.*, 10:2327–2341, 2004.

[32] C. Ciminelli, G. Granucci, and M. Persico. Are azobenzenophanes rotation–restricted? *J. Chem. Phys.*, 123:174317, 2005.

[33] M. Barbatti, G. Granucci, M. Persico, M. Ruckenbauer, M. Vazdar, M. Eckert-Maksić, and H. Lischka. The on-the-fly surface-hopping program system NEWTON-X: application to ab initio simulation of the nonadiabatic photodynamics of benchmark systems. *J. Photochem. Photobiol. A*, 190:228–240, 2007.

[34] P. de Sainte Claire. Molecular simulation of excimer fluorescence in polystyrene and poly(vinylcarbazole). *J. Phys. Chem. B*, 110:7334–7343, 2006.

[35] F. Santoro, A. Lami, R. Improta, and V. Barone. Effective method to compute vibrationally resolved optical spectra of large molecules at finite temperature in the gas phase and in solution. *J. Chem. Phys.*, 126:184102, 2007.

[36] E. Gindensperger, H. Koppel, and L. S. Cederbaum. Hierarchy of effective modes for the dynamics through conical intersections in macrosystems. *J. Chem. Phys.*, 126:034106, 2007.

[37] H. Satzger, C. Root, and M. Braun. Excited-state dynamics of trans- and cis-azobenzene after UV excitation in the $\pi\pi^*$ band. *J. Phys. Chem. A*, 108:6265–6271, 2004.

[38] T. Ishikawa, T. Noro, and T. Shoda. Theoretical study of the photoisomerization of azobenzene. *J. Chem. Phys.*, 115:7503–7512, 2001.

[39] C-W. Chang, Y-C. Lu, T-T. Wang, and E. W-G. Diau. Photoisomerization dynamics of azobenzene in solution with s_1 excitation: A femtosecond fluorescence anisotropy study. *J. Am. Chem. Soc.*, 126:10109–10118, 2004.

[40] L. Gagliardi, G. Orlandi, F. Bernardi, A. Cembran, and M. Garavelli. A theoretical study of the lowest electronic states of azobenzene: the role

of torsion coordinate in the cis-trans isomerization. *Theor. Chem. Acc.*, 111:363–372, 2004.

[41] A. Cembran, F. Bernardi, M. Garavelli, L. Gagliardi, and G. Orlandi. On the mechanism of the cis-trans isomerization in the lowest electronic state of azobenzene: S_0, S_1, T_1. *J. Am. Chem. Soc.*, 126:3234–3243, 2004.

[42] I. Conti, M. Garavelli, and G. Orlandi. The different photoisomeriation efficiency of azobenzene in the lowest $n\pi^*$ and $\pi\pi^*$ singlets: the role of a phantom state. *J. Am. Chem. Soc.*, 130:5216–5230, 2008.

[43] P. Cattaneo and M. Persico. An *ab initio* study of the photochemistry of azobenzene. *Phys. Chem. Chem. Phys.*, 1:4739–4743, 1999.

[44] E. W.-G. Diau. A new trans-to-cis photoisomerization mechanism of azobenzene on the s_1(n,π^*) surface. *J. Phys. Chem. A*, 108:950–956, 2004.

[45] H. Rau. *Photochromism. Molecules and systems*, chapter 4. Elsevier, Amsterdam, 1990.

[46] J. Otsuki, K. Suwa, K. Narutaki, C. Sinha, I. Yoshikawa, and K. Araki. Photochromism of 2-(phenylazo)imidazoles. *J. Phys. Chem. A*, 109:8064–8069, 2005.

[47] W. D. Cornell, P. Cieplak, C. I. Bayly, I. R. Gould, K. M. Merz Jr., D. M. Ferguson, D. C. Spellmeyer, T. Fox, J. W. Caldwell, and P. A. Kollman. A second generation force field for the simulation of proteins and nucleic acids. *J. Am. Chem. Soc.*, 117:5179–5197, 1995.

[48] M. Böckmann, C. Peter, L. Delle Site, N. L. Doltsinis, K. Kremer, and D. Marx. Atomistic force field for azobenzene compounds adapted for qm/mm simulations with applications to liquids and liquid crystals. *J. Chem. Theory Comput.*, 3:1789–1802, 2007.

[49] H. Heinz, R. A. Vaia, H. Koerner, and B. L. Farmer. Photoisomerization of azobenzene grafted to layered silicates: simulation and experimental challenges. *Chem. Mater.*, 20:6444–6456, 2008.

[50] S. A. Yuan, Y. S. Dou, W. F. Wu, Y. Hu, and J. S. Zhao. Why does trans-azobenzene have a smaller isomerization yield for $\pi\pi^*$ excitation than for $n\pi^*$ excitation? *J. Phys. Chem. A*, 112:13326–13334, 2008.

[51] L. Wang and X. Wang. Ab initio study of photoisomerization mechanisms of push-pull p, p'-disubstituted azobenzene derivatives on s_1 excited state. *J. Mol. Struct.:THEOCHEM*, 847:1–9, 2007.

[52] D. L. Cheung, S. J. Clark, and M. R. Wilson. Parametrization and validation of a force field for liquid-crystal forming molecules. *Phys. Rev. E*, 65:051709, 2002.

[53] R. Berardi, G. Cainelli, P. Galletti, D. Giacomini, A. Gualandi, L. Muccioli, and C. Zannoni. Can the π-facial selectivity of solvation be predicted by atomistic simulation? *J. Am. Chem. Soc.*, 127:10699–10706, 2005.

[54] R. Englman and J. Jortner. The energy gap law for radiationless transitions in large molecules. *Molec. Phys.*, 18:145–164, 1970.

[55] J. Jortner and D. Levine. *Photoselective Chemistry. Part I.* Adv. Chem. Phys. Wiley, New York, 1981.

[56] N. Kitamura, N. Sakata, H.-B. Kim, and S. Habuchi. Energy gap dependence of the nonradiative decay rate constant of 1-anilino-8-naphthalene sulfonato in reverse micelles. *Analytical Sciences*, 15:413–419, 1999.

[57] F. Ehlers, D. A. Wild, T. Lenzer, and K. Oum. Investigation of the s_1/ict $\rightarrow s_0$ internal conversion lifetime of 4′-apo-β-caroten-4′-al and 8′-apo-β-caroten-8′-al: dependence on conjugation length and solvent polarity. *J. Phys. Chem. A*, 111:2257–2265, 2007.

[58] S. Velate, X. Liu, and R. P. Steer. Does the radiationless relaxation of Soret-excited metalloporphyrins follow the energy gap law? *Chem. Phys. Lett.*, 427:295–299, 2006.

[59] J. von Neumann. Various techniques used in connection with random digits. *Appl. Math. Ser.*, 12:36–38, 1951.

[60] B. H. Besler, K. M. Merz Jr., and P. A. Kollman. Atomic charges derived from semiempirical methods. *J. Comput. Chem.*, 11:431, 1990.

[61] S. Kobayashi, H. Yokoyama, and H. Kamei. Substituent and solvent effects on electronic absorption spectra and thermal isomerization of push–pull–substitued *cis* azobenzenes. *Chem. Phys. Lett.*, 138:333–338, 1987.

[62] L. Briquet, D. P. Vercauteren, E. A. Perpète, and D. Jacquemin. Is solvated *trans*-azobenzene twisted or planar? *Chem. Phys. Lett.*, 417:190–195, 2006.

[63] T. Cusati, G. Granucci, M. Persico, and G. Spighi. Oscillator strength and polarization of the forbidden $n \rightarrow \pi^*$ band of *trans*-azobenzene: a computational study. *J. Chem. Phys.*, 128:194312, 2008.

[64] P. Procacci, E. Paci, T. Darden, and M. Marchi. Orac: a molecular dynamics program to simulate complex molecular systems with realistic electrostatic interactions. *J. Comput. Chem.*, 18:1848–1862, 1997.

[65] U. Essmann, L. Perera, M. L. Berkowitz, T. Darden, H. Lee, and L. G. Pedersen. A smooth particle mesh Ewald method. *J. Chem. Phys.*, 101:8577–8593, 1995.

[66] S. Nosé. A molecular dynamics method for simulations in the canonical ensemble. *Molec. Phys.*, 52:255268, 1984.

[67] W. G. Hoover. Canonical dynamics: Equilibrium phase-space distributions. *Phys. Rev. A*, 31:1695–1697, 1985.

[68] M. Parrinello and A. Rahman. Crystal structure and pair potentials: A molecular-dynamics study. *Phys. Rev. Letters*, 45:1196–1199, 1980.

[69] G. Granucci and M. Persico. Excited state dynamics with the trajectory surface hopping method: azobenzene and its derivatives as a case study. *Theor. Chem. Acc.*, 117:1131–1143, 2007.

[70] S. Malkin and E. Fischer. Temperature dependence of photoisomerization. part II. quantum yields of *cis*⇌*trans* isomerizations in azocompounds. *J. Am. Chem. Soc.*, 66:2482–2486, 1962.

[71] D. Gegiou, K. A. Muszkat, and E. Fischer. Temperature dependence of photoisomerization. VI. viscosity effect. *J. Am. Chem. Soc.*, 90:12–18, 1968.

[72] L. Creatini, T. Cusati, Granucci, and M. Persico. Photodynamics of azobenzene in a hindering environment. *Chem. Phys.*, 347:492–502, 2008.

[73] M. Poprawa-Smoluch M, J. Baggerman, H. Zhang, H. P. A. Maas, L. De Cola, and A. M. Brouwer. Photoisomerization of disperse red 1 studied with transient absorption spectroscopy and quantum chemical calculations. *J. Phys. Chem. A*, 110:11926–11937, 2006.

[74] T. Nägele, R. Hoche, W. Zinth, and J. Wachtveit. Femtosecond photoisomerization of *cis*-azobenzene. *Chem. Phys. Lett.*, 272:489–495, 1997.

[75] Y. Hirose, H. Yui, and T. Sawada. Effect of potential energy gap between the n–π^* and the π–π^* state on ultrafast photoisomerization dynamics of an azobenzene derivative. *J. Phys. Chem. A*, 106:3067–3071, 2002.

[76] Y. Zhang, R. M. Venable, and R. W. Pastor. Molecular dynamics simulations of neat alkanes: The viscosity dependence of rotational relaxation. *J. Chem. Phys.*, 100:2652–2660, 1996.

[77] R. E. Di Paolo, J. S. de Melo, J. Pina, H. D. Burrows, J. Morgado, and A. L. Maçanita. Conformational relaxation of *p*-phenylene-vinylene trimers in solution studied by picosecond time-resolved fluorescence. *ChemPhysChem*, 8:2657–2664, 2007.

[78] F. Serra and E. M. Terentjev. Effects of solvent viscosity and polarity on the isomerization of azobenzene. *Macromolecules*, 41:981–986, 2008.

[79] J. Shao, Y. Lei, Z. Wen, Y. Dou, and Z. Wang. Nonadiabatic simulation study of photoisomerization of azobenzene: detailed mechanism and load-resisting capacity. *J. Chem. Phys.*, 129:164111, 2008.

[80] M. Böckmann, N. L. Doltsinis, and D. Marx. Azobenzene photoswitches in bulk materials. *Phys. Rev. E*, 78:036101, 2008.

[81] Y.-C. Lu, C.-W. Chang, and E. W.-G. Diau. Femtosecond fluorescence dynamics of *trans*–azobenzene in hexane on excitation to the $s_1(n, \pi^*)$ state. *J. Chin. Chem. Soc.*, 49:693–701, 2002.

[82] T. Schultz, J. Quenneville, B. Levine, A. Toniolo, T. J. Martinez, S. Lochbrunner, M. Schmitt, J. P. Shaffer, M. Z. Zgierski, and A. Stolow.

Mechanism and dynamics of azobenzene photoisomerization. *J. Am. Chem. Soc.*, 125:8098–8099, 2003.

[83] C. M. Stuart, R. R. Frontiera, and R. A. Mathies. Excited-state structure and dynamics of *cis*- and *trans*-azobenzene from resonance Raman intensity analysis. *J. Phys. Chem. A*, 111:12072–12080, 2007.

[84] P. Hamm, S. M. Ohline, and W. Zinth. Vibrational cooling after ultrafast photoisomerization of azobenzene measured by femtosecond infrared spectroscopy. *J. Phys. Chem*, 106:519–529, 1997.

[85] A. Toniolo, C. Ciminelli, M. Persico, and T. J. Martinez. Simulation of the photodynamics of azobenzene on its first excited state: Comparison of full multiple spawning and surface hopping treatments. *J. Chem. Phys.*, 123:234308, 2005.

[86] G. Granucci and M. Persico. Critical appraisal of the fewest switches algorithm for surface hopping. *J. Chem. Phys.*, 126:134114, 2007.

[87] I. K. Lednev, T.-Q. Ye, P. Matousek, M. Towrie, P. Foggi, F. V. R. Neuwahl, S. Umapathy, R. E. Hester, and J. N. Moore. Femtosecond time-resolved uv-visible absorbtion spectroscopy of *trans*-azobenzene on excitation wavelength. *Chem. Phys. Lett.*, 290:68–74, 1998.

[88] T. Fujino and T. Tahara. Femtosecond time-resolved Raman study of *trans*-azobenzene. *J. Phys. Chem. A*, 104:4203–4210, 2000.

[89] J. G. Baragi and M. I. Aralaguppi. Excess and deviation properties for the binary mixtures of of methylcyclohexane with benzene, toluene, p-xylene, mesitylene, and anisole at T=(298.15, 303.15, and 308.15) K. *J. Chem. Thermodynamics*, 38:1717–1724, 2006.

Table 1: Selected physical properties of the solvents studied: experimental viscosities (cP), densities (g cm^{-3}), boiling temperatures (K), calculated densities (g cm^{-3}), and molecular dipoles (D).

solvent		$\rho^{(a)}$	$\eta^{(a)}$	$T_b^{(a)}$	$\rho^{(b)}$	$\mu^{(c)}$
n-hexane	(HEX)	0.659	0.289	342	0.62	0.00
toluene	(TOL)	0.867	0.538	384	0.89	0.34
ethanol	(ETH)	0.789	1.005	352	0.75	1.53
anisole	(ANI)	0.989	1.008	427	1.02	1.06
ethylene glycol	(EGL)	1.114	14.38	470	1.06	0.00

[(a)] Experimental values. Data for ANI (at 298.15 K) have beeb taken from reference [89], while for ETH, EGL, HEX, TOL (at 293 K) the source was the Korea Thermophysical Properties Data Bank (URL http://www.cheric.org/research/kdb/).
[(b)] Calculated from a MD simulation of a model solution of 99 solvent molecules and 1 AB solute, at $T = 300$ K, and $P = 1$ bar.

[(c)] Computed in vacuum for an isolated molecule at B3LYP//6–31G** level.

Table 2: Simulated (Φ_{MD}, this work) and experimental (Φ_{exp}, assigned using the solvent classification proposed in table 1 of reference [69]) $n\pi^*$ quantum yields; average lifetimes of the excited state (overall τ_{S_1}, and specific for *trans* and *cis* products only $\tau_{S_1,cis}$, $\tau_{S_1,trans}$); parameters obtained by fitting the S_1 population with the decay model $P_{S_1}(t) = a_1 \exp(-(t-\tau_0)/\tau_1) + a_2 \exp(-(t-\tau_0)/\tau_2)$ discussed in the text. All times are expressed in picoseconds.

property	VAC	HEX	TOL	ETH	ANI	EGL
Φ_{exp}	0.46	0.20-0.27	0.21-0.28	0.20-0.36	0.21-0.28	0.20-0.42
Φ_{MD}	0.52	0.24	0.23	0.24	0.20	0.16
τ_{S_1}	0.44	2.11	2.42	1.98	2.70	5.30
$\tau_{S_1,cis}$	0.46	2.04	2.35	2.00	2.87	4.74
$\tau_{S_1,trans}$	0.42	2.13	2.44	1.98	2.65	5.41
τ_0	0.18	0.28	0.28	0.26	0.27	0.31
$\tau_1^{(a_1)}$	$0.26^{(1.0)}$	$0.94^{(0.4)}$	$0.45^{(0.2)}$	$0.50^{(0.2)}$	$0.83^{(0.3)}$	$0.30^{(0.1)}$
$\tau_2^{(a_2)}$	-	$1.17^{(0.6)}$	$1.70^{(0.8)}$	$1.38^{(0.8)}$	$1.67^{(0.7)}$	$4.50^{(0.9)}$

Table 3: Typical correlation times for the rotational dynamics of azobenzene (τ_r, ps) during the photoisomerization for *cis* and *trans* final products, estimated from the decay time of the autocorrelation function of the N=N bond orientation.

time /ps	VAC	HEX	TOL	ETH	ANI	EGL
$\tau_{rot,cis}$	2.3	6.9	11.8	11.8	22	720
$\tau_{rot,trans}$	2.1	5.8	7.6	7.4	11	364

Table 4: The isomerization pathway classification in vacuum and in the different solvents. For each patway, the fraction of trajectories reaching the maximum value of θ in the excited state is reported between parentheses.

mechanism	VAC	HEX	TOL	ETH	ANI	EGL
torsion	$0.56^{(0.32)}$	$0.24^{(0.38)}$	$0.27^{(0.40)}$	$0.30^{(0.28)}$	$0.28^{(0.36)}$	$0.24^{(0.31)}$
mixed	$0.43^{(0.01)}$	$0.67^{(0.00)}$	$0.66^{(0.01)}$	$0.64^{(0.01)}$	$0.65^{(0.01)}$	$0.64^{(0.01)}$
inversion	$0.01^{(0.00)}$	$0.09^{(0.00)}$	$0.07^{(0.00)}$	$0.06^{(0.00)}$	$0.07^{(0.00)}$	$0.11^{(0.00)}$

Table 5: The n, π^* *trans–cis* photoisomerization quantum yield Φ and the lifetime τ_{S_1} computed from N experiments in vacuum and *n*–hexane using different sets of the empirical parameters K and χ (c. f. equation 3).

K	χ	vacuum			hexane		
fs^{-1}	mol $kcal^{-1}$	Φ	τ_{S_1} /ps	N	Φ	τ_{S_1} /ps	N
reference		0.46[a]	0.5[a]	200	0.20-0.27[b]	1-3[c]	-
0.01	0.10	0.36	0.46	100	0.09	0.67	100
0.01	0.50	0.37	1.85	100	-	-	-
0.10	0.10	0.02	0.26	100	-	-	-
0.10	0.60	0.55	0.51	100	0.10	0.85	100
1.00	1.00	0.48	0.40	100	-	-	-
1.00	1.50	0.47	1.30	100	-	-	-
2.00	1.00	0.32	0.36	100	-	-	-
2.00	1.20	0.56	0.40	100	-	-	-
2.00	1.30	0.50	0.51	100	0.18	0.95	100
4.00	1.00	0.20	0.33	100	-	-	-
4.00	1.50	0.58	0.51	100	0.19	0.92	100
4.00	1.85	0.52	1.20	100	0.20	2.3	400
5.00	0.50	0.02	0.29	100	-	-	-
5.00	1.00	0.18	0.34	100	-	-	-
5.00	1.40	0.52	0.41	200	0.17	0.82	100
5.00	1.50	0.54	0.45	1500	0.15	0.98	100
5.00	1.60	0.55	0.53	1500	0.16	1.1	200
5.00	1.90	0.49	1.05	100	0.24	2.1	1500
5.00	2.00	0.61	1.32	100	0.24	2.6	200
5.00	2.50	0.29	6.66	100	-	-	-

[a] Simulation value, reference [85].
[b] Experimental range for aliphatic solvents, reference [69]).
[c] Experimental range from references [87, 88, 81, 39, 83].

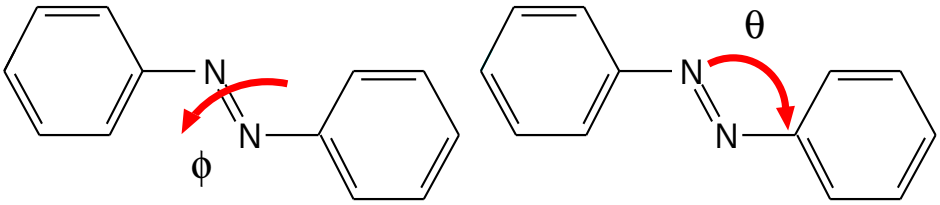

Figure 1: Scheme of the azobenzene (AB) molecule showing the *Ph*-*N*=*N*-*Ph* torsional angle ϕ, and the *Ph*-*N*=*N* bending angle θ.

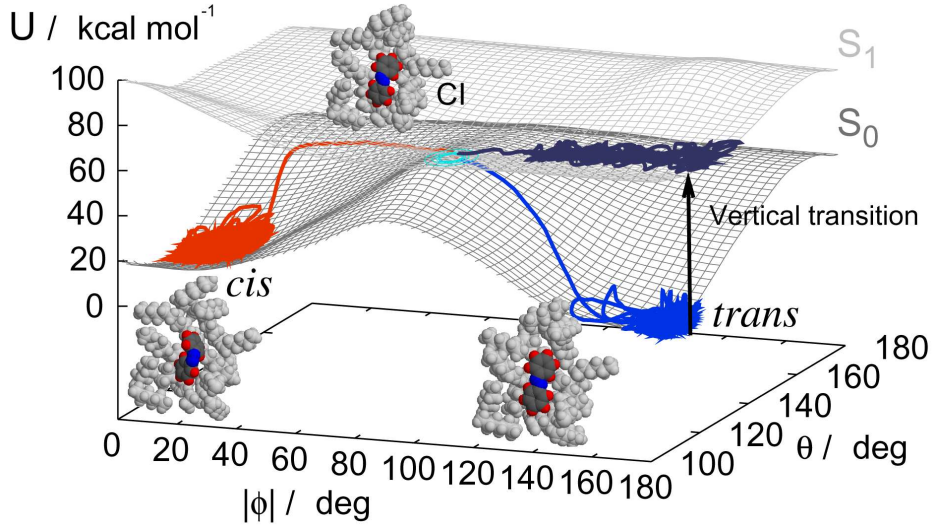

Figure 2: The potential energy surfaces for the S_0 and S_1 states of AB used in this work [38], with three superimposed representative MD trajectories: in the excited state (black), after one successful (red), and one unsuccessful (blue) isomerization process of AB in *n*–hexane. We also show snapshots of an AB molecule with the closest solvent neighbors in typical MD configurations for the *trans*, *cis*, and CI states.

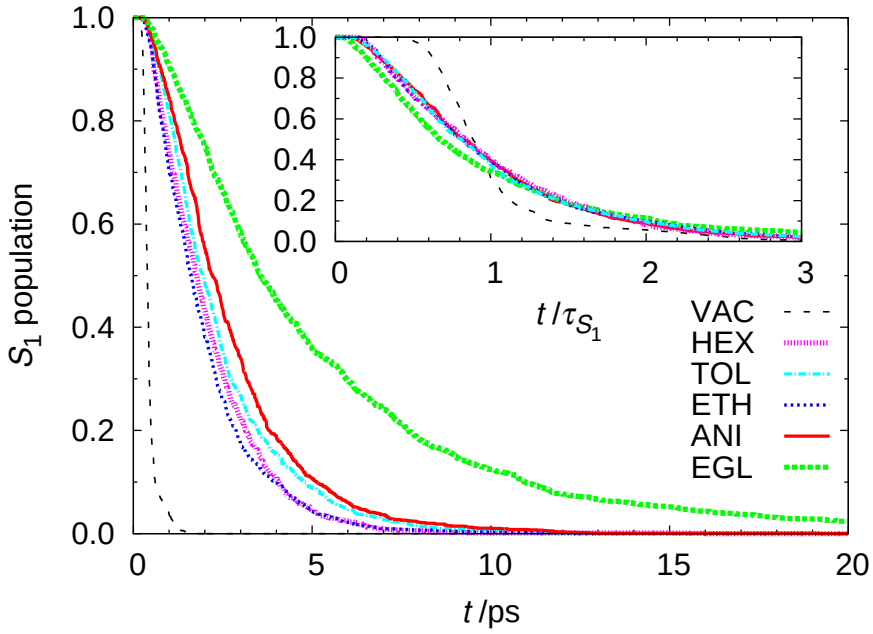

Figure 3: Time evolution of the population of the excited state S_1. In the inset, the same data plotted against reduced time units t/τ_{S_1} allow to appreciate the qualitative difference between the behaviour in vacuum and in solvents.

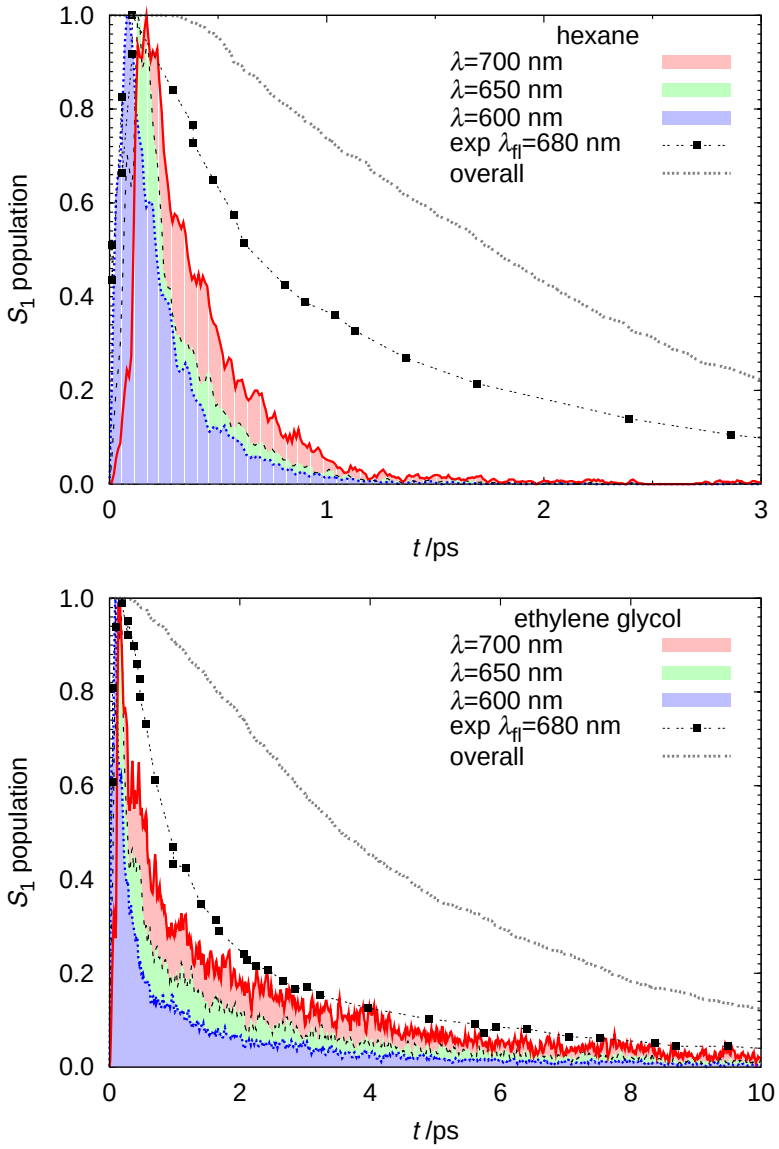

Figure 4: Time evolution of the population of the excited state S_1 (arbitrary units) as function of the energy difference with the ground state S_0 (nanometers), computed in vacuum, *n*-hexane and ethylene glycol. Each color identifies the population in a 50 nm window centered at the indicated wavelength. Experimental profiles have been taken from reference [39]

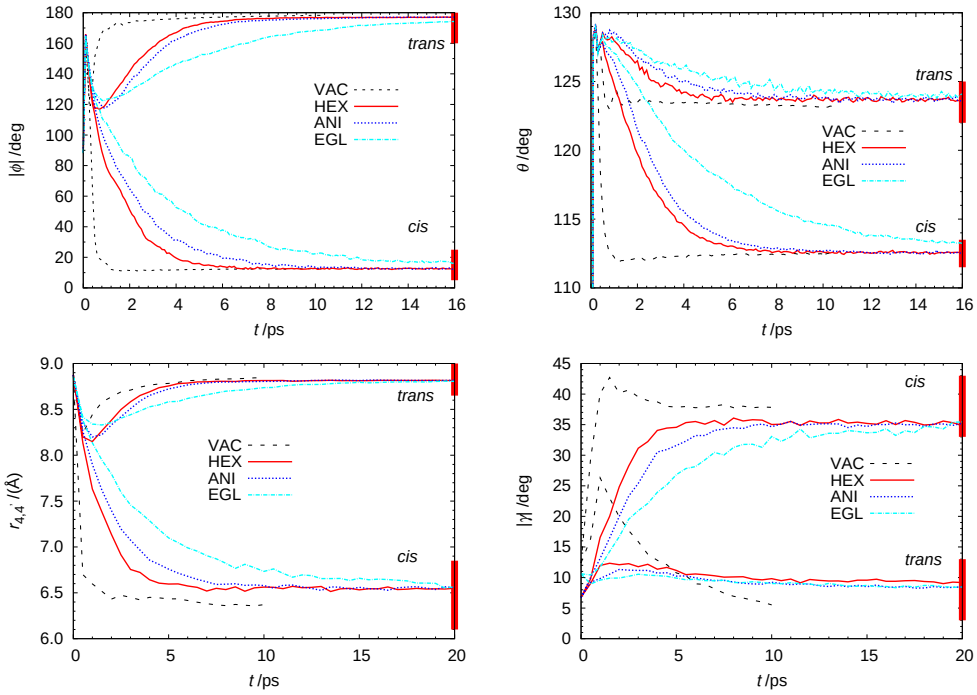

Figure 5: The evolution of conformational indicators, separately averaged according to the final isomerization product (indicated at the right edges of the plots): [a] *Ph*-*N*=*N*-*Ph* torsional angle $|\phi|$; [b] *N*=*N*-*C* bending angles θ; [c] phenyl-phenyl distance $r_{4,4'}$; and [d] *C*-*C*-*N*=*N* torsional angles $|\gamma|$.

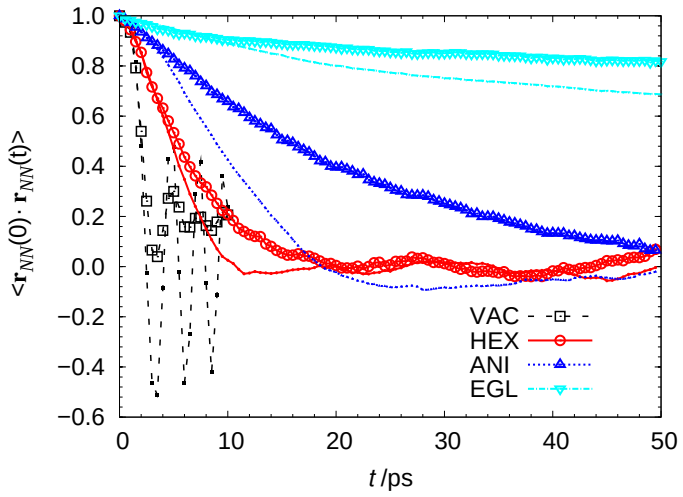

Figure 6: Time autocorrelation function of the azo bond unit vector $\langle \mathbf{r}_{NN}(0) \cdot \mathbf{r}_{NN}(t) \rangle$. The average values from trajectories leading to *cis* isomers are marked with large empty symbols, while those for trajectories leading to *trans* isomers are plotted with small filled symbols.

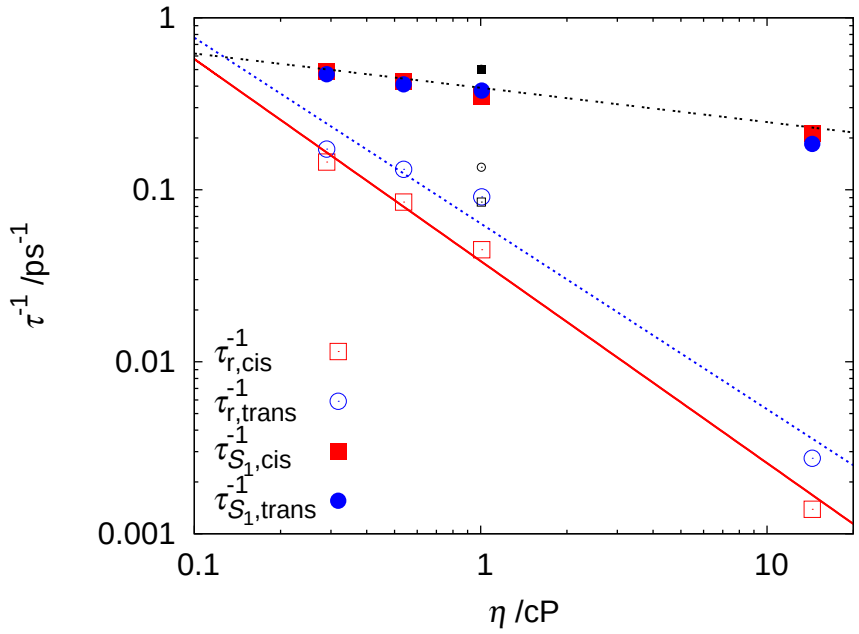

Figure 7: Log-log plot of the simulated rotational relaxation rate constant $(1/\tau_r)$ and of the excited state relaxation rate constant $(1/\tau_{S_1})$ versus experimental viscosities η for *cis*- (red squares) and *trans*-azobenzene (blue circles). The straigth lines represent the fit with the equation $\tau^{-1} = A\eta^{-\alpha}$ (black dotted line: $A_{S_1} = 0.39$, $\alpha_{S_1} = 0.2$; red line:$A_{r,cis} = 0.039$, $\alpha_{r,cis} = 1.17$; blue dotted line: $A_{r,trans} = 0.064$, $\alpha_{r,trans} = 1.08$). The times in ethanol, omitted from the fits, are shown in black.

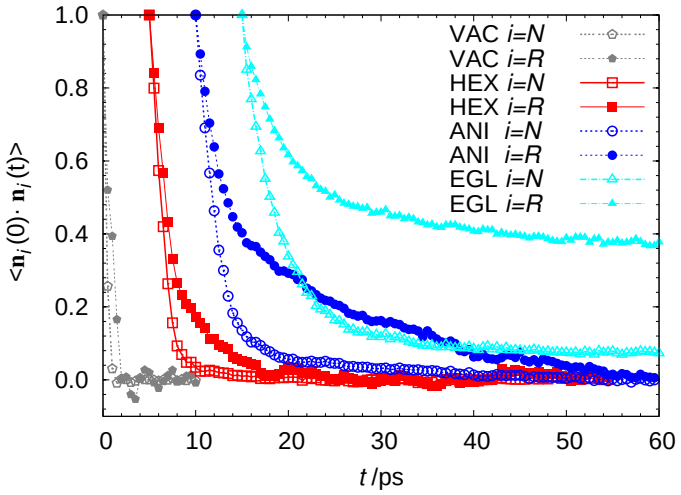

Figure 8: Time autocorrelation function $\langle \mathbf{n}_i(0) \cdot \mathbf{n}_i(t) \rangle$ of the normals to the phenyl ring planes (i=R, filled symbols) and the planes containing C-N=N atoms (i=N, $\mathbf{n}_N = \hat{\mathbf{r}}_{CN} \times \hat{\mathbf{r}}_{NN}$, empty symbols). For better visualization, the time origins for HEX (squares), ANI (circles) and EGL (triangles) have been shifted with respect to VAC (pentagons) of 5, 10 and 15 ps respectively. Simulation data have been averaged on the two possible planes for N and R, and only on the trajectories leading to the *cis* isomer.

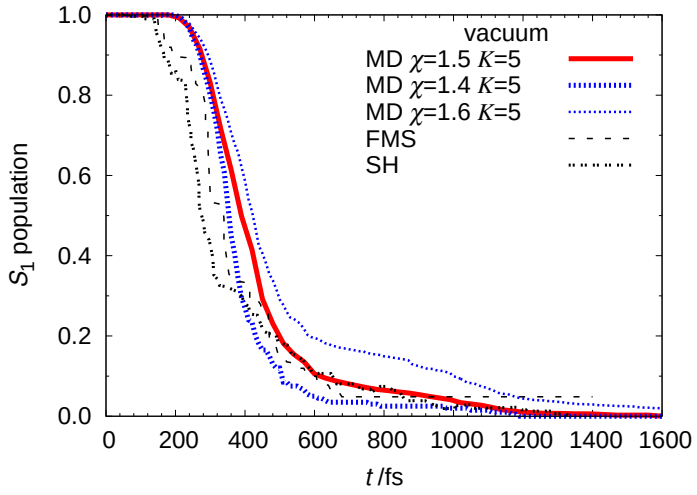

Figure 9: Time evolution of the population of AB excited state S_1 in vacuum, as function of the empirical parameters K and χ (in fs^{-1} and mol kcal^{-1} respectively). The FMS and TSH simulation results of Persico and coworkers[31, 85] are also shown for comparison.

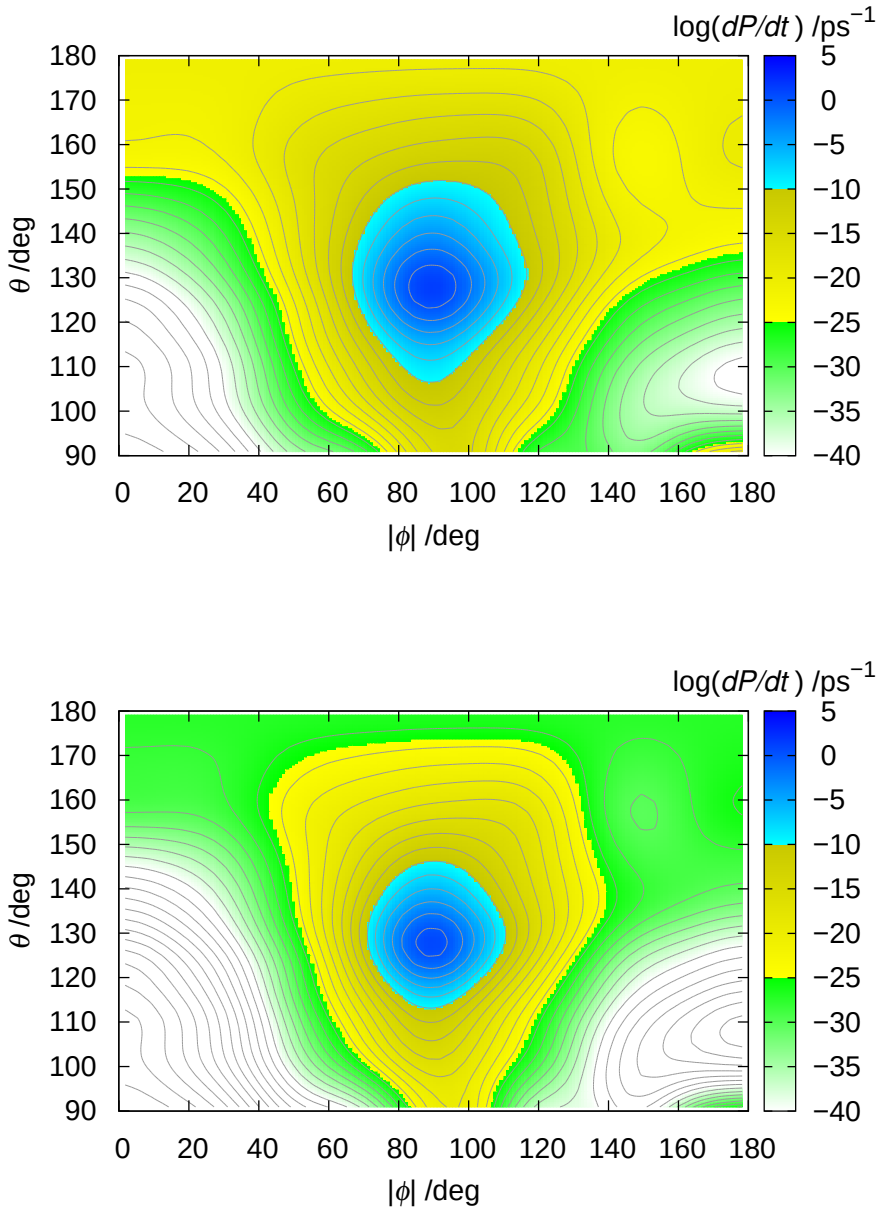

Figure 10: The decay probability rate maps calculated with equation 3, using the optimal parameters for vacuum ($K = 5$ fs^{-1}, $\chi = 1.5$ mol kcal^{-1}, top) and for solvents ($K = 5$ fs^{-1}, $\chi = 1.9$ mol kcal^{-1}, bottom). Level lines are separated by two orders of magnitude.